MAGNETIC STRUCTURE

OF

MANGANESE PYROPHOSPHATE

DETERMINATION OF THE MAGNETIC STRUCTURE

OF

MANGANESE PYROPHOSPHATE $Mn_2P_2O_7$ BY NEUTRON DIFFRACTION

By

GURNAM SINGH GILL

A Thesis

Submitted to the Faculty of Graduate Studies

in Partial Fulfilment of the Requirements

for the Degree

Master of Science

MASTER OF SCIENCE (1971)
(Physics)

McMASTER UNIVERSITY
Hamilton, Ontario

TITLE: Determination of the Magnetic Structure of Manganese Pyrophosphate $Mn_2P_2O_7$ by Neutron Diffraction.

AUTHOR: Gurnam Singh Gill, B.Sc. Hon. (University of Surrey, U.K.)

SUPERVISOR: Professor M. F. Collins

NUMBER OF PAGES: 45

SCOPE AND CONTENTS: Magnetic Structure of antiferromagnetic $Mn_2P_2O_7$ at 4.2° K has been established by neutron diffraction from a powder specimen. The magnetic unit cell is found to be the same size as the chemical unit cell. The spins are arranged in ferromagnetic sheets with the moments in each sheet aligned antiferromagnetically relative to its adjacent sheets. Neutron diffraction results in regard to the critical temperature, $(13\pm3)^\circ$ K, and the spins being at an angle of 23° from the a-axis in the a-c plane have been found consistent with the ones obtained by Fowlis, Atkinson, Choh and Stager by susceptibility and NMR studies on the material. However, to confirm the angle with some precision, more work, probably with a single crystal, will be required.

ACKNOWLEDGEMENTS

I would like to thank Dr. M. F. Collins and Dr. C. Stager for their valuable help and guidance at all levels while this research was being carried out.

Also, I wish to thank Dr. C. Calvo and Mr. V. K. Tondon for making available X-ray data on the lattice parameters of Manganese pyrophosphate at low temperature. And finally, my thanks are due to Miss Davies for typing the manuscript and helping with the figures.

This research was supported by the National Research Council of Canada and by an Alfred P. Sloan Fellowship for Dr. M. F. Collins.

TABLE OF CONTENTS

LIST OF FIGURES

(List of Figures continued)

(List of Figures continued)

LIST OF TABLES

I INTRODUCTION

A ferromagnet has all its spins aligned in a given direction at low temperatures and thus possesses a spontaneous magnetic moment. For ferromagnetism to exist in a material consisting of only one type of atoms, not only should the atoms have net magnetic moments but also have a positive exchange integral. A positive exchange integral is necessary for co-operative interaction between spins to take place and to result in a state of lowest energy. In the case of materials composed of more than one type of atoms, the exchange integral is predominantly positive. A negative exchange integral is, however, possible for many non-ferromagnetic substances diluted with a certain concentration of magnetic atoms. For these, the lowest energy state is obtained by the occurrence of maximum number of antiparallel pairs. The concept in question is illustrated in the following paragraph for a material consisting of two types of atoms, and can be extended to more complex structures.

Visualize a crystalline structure consisting of two interpenetrating sub-lattices such that atoms on one lattice have, for their nearest neighbours, atoms only on the other lattice. Further, postulating a negative exchange integral and nearest neighbour interaction only, it is feasible, theoretically, for such a structure to exhibit a Curie temperature. Below the Curie temperature, the magnetization versus temperature curves for each sub-lattice are similar to those of an ordinary ferromagnetic substance but with the proviso

that the direction of magnetization on one is antiparallel to that on the other lattice. This will result in zero spontaneous magnetization. Above the Curie temperature, the material behaves like a paramagnetic because the thermal energy is sufficient to destroy the anti-parallel ordering of the magnetic moments on the atoms. Materials displaying such characteristics are termed antiferromagnetic.

It is now known that most of the antiferromagnetic compounds are ionic crystals, e.g. MnO, MnF_2, etc. In these substances the cations i.e. the magnetic ions are separated by the anions, e.g. O or F. Shull and others have, through neutron diffraction experiments, established the existence of a strong antiferromagnetic coupling between the next to nearest magnetic ions via the large intervening anions. Certain magnetically diluted salts also reveal the presence of similar indirect exchange interactions. The interaction is known as super-exchange. The importance of this superexchange in antiferromagnetic substances was first emphasized by Bizette and Neel, while theoretical justifications for the mechanism were provided by Anderson and Van Vleck.

In order to illustrate the operation of the mechanism of super-exchange, a simple example by Anderson is cited. He isolates two cations e.g. Mn^{++} which are separated, say, by O^{--}. Suppose there are two electrons in the p-orbital of the O ion while the Mn ions have one electron in each of their d-orbitals. Anderson says that one can imagine the possibility of a transfer of one of the electrons from O^{--}. to one of the Mn ions, thus, giving rise to an excited state. The other unpaired electron on O^{--} can then pair with the second Mn ion. There should be strong interaction between the two electrons now on the first Mn ion. Also the two electrons on the O ion have opposite

spins and will lead to the appearance of indirect coupling between the two Mn ions through this excited state. Similar exchange interaction can be imagined to be occurring between the Mn^{++} in $Mn_2P_2O_7$ through the intervening O and possibly through a combination of O and P ions together which may lead to an ordered state below the Neel temperature. Fowlis and Stager have proved it to be so.

As for the spin arrangement in $Mn_2P_2O_7$, Fowlis and Stager and Atkinson and Stager have found from susceptibility and NMR measurements that it was antiferromagnetic below 14°K with the spins aligned in the a-c plane at an angle of 23° with the a-axis. Choh and Stager, by conducting NMR studies on the compound in the ordered state have not only confirmed the spin direction but also attempted to deduce from symmetry considerations, the possible spin arrangements. They conclude that four such configurations are compatible with the chemical unit cell, doubled along the C-axis. The present work is aimed at establishing the magnetic structure of the compound by employing neutron diffraction measurements on a powdered sample.

II THEORY OF NEUTRON DIFFRACTION

A. General

A neutron with an equivalent wave-length comparable to the internuclei distance of a 3-dimensional periodic array of nuclei, e.g. in a crystal, will be scattered in a similar fashion as the X-rays are by electrons under the same conditions. Scattering can be elastic or inelastic but we shall be concerned with the former only. Further, elastic scattering can be coherent and incoherent, but it is coherent scattering which is made use of in taking various measurements on the diffracted beam. The reason being that interference effects can occur producing intensity redistributions in the diffracted beam. For a given wave-length λ, the positions of the various reflections from planes (h,k,l) are governed by the familiar Bragg law;

$$2d_{hkl} \text{ Sin } \theta = n\lambda \quad \text{(i)}$$

where d_{hkl} is the spacing of (h,k,l) planes. In the case of a polycrystalline powdered sample, which was used in the present experiment, only the crystallites oriented at the correct angle to the incident beam will obey (i) and contribute to coherent scattering. Diffracted beam will leave the specimen along the generators of cones concentric with the incident beam. The generators will make an angle 2θ with the direction of the original beam. In order to compute the intensity of the scattered beam, one would need to know the nuclear structure factor $F_{nuclear}$ given by the following relation.

$$F^2_{nuclear} = \left| \sum b \exp 2\pi i \, (hx + ky + lz) \right|^2 \qquad \text{(ii)}$$

Where b is the coherent nuclear scattering amplitude for each type of atom; x,y,z are the fractional co-ordinates of the atoms, and the summation is carried over all the atoms in the unit cell.

B. Magnetic Scattering

A neutron is known to possess a spin $\frac{1}{2}$ and a magnetic moment of 1.9 nuclear magnetons. Systems with resultant magnetic moments will, thus, interact with the neutron through its magnetic moment. For example, the elements of the first transition series, which includes Mn, have incomplete 3-d shells. This means the atoms will have unpaired electron spins resulting in net magnetic moments on the atoms. Consequently, contribution to neutron scattering from these atoms will be both nuclear and magnetic. However, due to the extended charge distributions of the outer unpaired electrons, magnetic scattering will exhibit a form factor variation. In the ordered state, there will be coherent scattering of neutrons by the various magnetic ions in the material. In this case, the scattering amplitude p will be given by;

$$p = \left(\frac{e^2 \gamma}{2mC^2} \right) \qquad 2Sf \qquad \text{(iii)}$$

Where,

e = electronic charge

m = electron mass

γ = magnetic moment of neutron in nuclear magnetons

C = velocity of light

2S = magnetic moment in Bohr magnetons of the atom in which orbital moment is completely quenched

f = form factor

The magnetic structure is calculated in a similar manner as the nuclear one, and is given by the following relation.

$$F^2_{magnetic} = \left| \Sigma p \exp 2\pi i (hx + ky + lz) \right|^2 \quad \text{(iv)}$$

Where p is defined in (iii) and the summation runs over all the magnetic atoms in the magnetic unit cell.

C. Intensities

For coherent elastic scattering the intensities of the Bragg reflections will be proportional to the square of the total structure factor. In the case of the unpolarized neutrons, there will be no cross terms, and thus, the square of the resultant structure factor F^2_{hkl} will be the sum of the squares of the nuclear and magnetic structure factors

or, $$F^2_{hkl} = F^2_{nuclear} + q^2 F^2_{magnetic}$$

Here, q is known as the magnetic interaction vector and is defined as:

$$\underline{q} = \underline{\epsilon}(\underline{\epsilon} \cdot \underline{k}) - \underline{k}$$

$\underline{\epsilon}$ and $\underline{k}$ are unit vectors and are defined in fig. (I). It follows that

$$q^2 = 1 - (\underline{\epsilon} \cdot \underline{k})^2$$

Thus using the above relations, one can calculate the Bragg angles and intensities of various reflections. Since there will be a number of equivalent planes for a certain (h,k,l) reflection, $F^2_{nuclear}$ and $F^2_{magnetic}$ must be multiplied by the appropriate multiplicity factor j. For a rectangular container, assuming negligible absorption,

$$I_{nuclear} = \text{constant} \times \frac{j F^2_{nuc}}{\sin^2 2\theta}$$

$$I_{magnetic} = \text{constant} \times \frac{j F^2_{magnetic}}{Sin^2 2\theta}$$

where, I denotes intensity for a particular h,k,l combination.

III CRYSTALLOGRAPHY

Chemically $Mn_2P_2O_7$ belongs to a family of divalent metal pyrophosphates like $Co_2P_2O_7$, $Cu_2P_2O_7$ and $Mg_2P_2O_7$. It is known to possess a monoclinic symmetry with the space group C_2/m (Lukaszewicz and Smajkiewicz). Crystallographic investigations show that unlike other pyrophosphates, it does not display a high or low temperature phase change. At room temperature, the lattice parameters are:

$a = 6.624$ A°; $b = 8.579$ A°; $c = 4.539$ A°; $\beta = 102.74$ °

Changes occurring in a, b, c, and β at liquid nitrogen temperature (Calvo and Tondon, private Communications) are as follows:

$$\Delta a = -0.4\%$$

$$\Delta b = -0.25\%$$

$$\Delta c = -0.5\%$$

$$\Delta \beta = < 1'$$

Thus the changes in lattice parameters at 77°k are less than 0.5% and almost negligible.

The unit cell of Manganese pyrophosphate contains two molecules and has 4 equivalent Mn ions and 4 equivalent phosphorus ions. The structure is known to consist of sheets of Mn ions separated by those of $(P_2O_7)^{4-}$ anions. Each Manganese ion is surrounded by an approximate octahedron of oxygen ions and is situated on a two fold rotation axis; whereas the phosphorus ions are separated by a mirror plane. A projection of the unit cell on the a-b plane is shown in fig. (II). Appropriate fractional distances

are also given.

IV MATERIAL AND APPARATUS

A. Material

$Mn_2P_2O_7$ powder was prepared using the technique described by Atkinson and Stager. The powder was heated to 200°C for three hours to drive off the water of crystallization. It was then transferred to an air tight container.

B. Apparatus

a) Cryostat: A variable temperature cryostat designed and assembled by Sulfrian Cryogenics for neutron diffraction work was used to cool $Mn_2P_2O_7$ powder down to liquid Nitrogen and liquid Helium temperatures. An outline of the cryostat is traced in fig. (III).

b) Sample Container fig. (IV) : It was an inch diameter and half an inch long Aluminium tube machined out of a solid piece. One of its ends was closed permanently while the other had a removable flap on it. The thickness of the walls was 0.015 in. A two inch threaded Brass bar was fitted to the container so that it could be attached to the lower end of RR (fig. III) in the cryostat. The Brass bar was covered in Cd. sheet to avoid any spurious scattering taking place.

c) McMaster University Triple Axis Spectrometer (Brockhouse et al.): The instrument can be programmed to run in a count, print and move cycle. A He-3 counter, moving in steps of 0.1° or larger

scans the diffracted beam, and can be set to count either for a preset monitor count or time. After the required interval, a print-out of signal or time, the number of counts registered by the counter, and if desired, the background counts is given. The counter then moves another step. The monochromator was a Copper crystal with its (220) planes facing the white beam at 49° and thus, diffracted neutrons of 1.06 A° wave-length. A general outlay of the whole set-up is drawn in fig. (V). The spectrometer was run in two-axis mode of operation and was found to have a resolution of 0.7° full width at half height.

V EXPERIMENTAL PROCEDURE

Surveys of the level of background scattering around the instrument were conducted and appropriate precautionary measures such as the provision of Cadmium and wax shielding were taken to minimise the effects as much as possible. To cut down the unnecessary contributions to background scattering, dimensions of the beam were limited to $1\frac{1}{2}$ in. x 1 in. by inserting a similiar sized slit cut in a Cadmium sheet.

After these precautions and adjustments, a Copper powder sample was put in the neutron beam and a pattern was obtained. This was used to establish the straight-through position (fig. V) and to confirm the neutron wave-length, since the d-spacings and positions of the lines were known for Copper.

Measurements of wave-length and reference position were followed by putting the cryostat in the beam with the container packed with $Mn_2P_2O_7$ powder mounted in position. Height of the container was adjusted so that it was fully bathed in the beam. The sample chamber was flushed with Helium gas in order to drive out air and water vapour, and was then sealed.

The counter was set to scan the scattered beam in steps of 0.2° for ten thousand (15 minutes)monitor counts per step. Such runs were conducted at 300° K, 77° K and 4.2° K, respectively. In order to assess the extent of the contributions to background scattering due to scattering from cold Helium gas, the container and the walls of the

cryostat, the scanning procedure was repeated with the empty container at the afore-mentioned temperatures. Results are tabulated and discussed in the next two sections.

VI RESULTS

A. Diffraction Patterns

Plots of averaged intensity at 77°K and 4.2°K in terms of neutrons scattered into the counter per 15 minutes versus angle of scattering 2θ are depicted in figs. (VI) and (VII) respectively. Scattering due to the empty container and cold Helium gas was subtracted beforehand from the total scattering. The pattern at 300°K is not shown because it was exactly similar to the one at 77°K. For a direct comparison of the respective patterns at liquid He and liquid N_2 temperatures, the two curves are presented together in fig. (VIII). One cannot fail to notice the appearance of extra lines at 4.2°K. To characterize these lines, the counter was placed at 7.1° where a strong line was observed. Temperature was allowed to rise and counts were recorded every 10 minutes. A plot of neutron intensity versus temperature is shown in fig. (IX) and the results are discussed in Section (VII).

B. Interplanar Spacing and Structure Factors

(i) Interplanar Spacing: For a monoclinic system, interplanar spacing, d_{hkl}, was worked out using the relationship,

$$d_{hkl}^{-2} = \frac{h^2/a^2 + l^2/c^2 - 2hl\cos\beta/ac}{\sin^2\beta} + \frac{k^2}{b^2}$$

Where,

a) h,k,l were the Miller indices of the various planes.

b) a,b,c were the lattice parameters of the unit cell.

c) β was the angle between a and c.

Thus, knowing d_{hkl}, the corresponding Bragg angle could be calculated from (i).

ii) Structure Factors: Nuclear and magnetic structure factors were computed using equations (ii) and (iv) respectively.

a) Nuclear Structure factor: Equation (ii)(Section II) can be written as

$$F_{nuclear} = b\left[\cos 2\pi (hx + ky + lz) + i \operatorname{Sin} 2\pi (hx + ky + lz)\right]$$

Various symbols are explained in section II.

There are 4 Manganese, 4 Phosphorus and 14 oxygen atoms in the cell. After substituting for the position of each atom in the above expression for $F_{nuclear}$ and simplifying, it can be written as

$$\begin{aligned} F_{nuclear} = \operatorname{Cos}^2 \frac{\pi}{2}(h + k)\Big[&4b_{Mn} \cos \pi l \cos 2\pi (0.3105)k \\ &+ 4b_P \cos 2\pi (0.2150h + 0.90791) + 2b_O \\ &+ 4b_O \cos 2\pi (0.3764h + 0.20941) \\ &+ 8b_O \cos 2\pi (0.2183h + 0.72521) \cos 2\pi (0.1488k)\Big] \end{aligned}$$

For (h + k) odd, $F_{nuclear} = 0$; which is a result of C-face centering.

For (h + k) even, the above relation reduces to

$$\begin{aligned} F_{nuclear} = 2\Big[&2b_{Mn} \cos 180l \cos 11.8k + 2b_p \cos (77.4h + 326.81) \\ &+ b_O\Big\{1 + 2 \cos (135.5h + 75.41) \\ &+ 4 \cos (78.6h + 261.11) \cos 53.6h\Big\}\Big] \end{aligned}$$

Where, $b_{Mn} = -0.36$; $b_p = 0.53$; $b_0 = 0.577$ in units of 10^{-12} cm.

Results are tabulated in table I.

(ii) Magnetic Structure Factor: Like (ii), (iv) can be written as

$$F_{magnetic} = \sum_{i=1}^{4} p_i \left[\cos 2\pi (hx + ky + lz) + i \operatorname{Sin} 2\pi (hx + ky + lz).\right]$$

There are four Manganese ions in the cell situated at

(1) $o, y, \frac{1}{2}$

(2) $\frac{1}{2}, (y + \frac{1}{2}), \frac{1}{2}$

(3) $0, (-y), \frac{1}{2}$

(4) $-\frac{1}{2}, (-\frac{1}{2}-y), \frac{1}{2}$

with $y = 0.31$.

Since the structure is periodic, it is possible to redefine the cell zero in a desired manner. If we put 4 spins in a plane with the Z-co-ordinate zero, then it will be easier to add in the Z-co-ordinate for the spins above the ones with Z = 0. Thus, for the spins having Z = 0,

$$F_{magnetic} = (p_1 + p_3) \cos 2\pi ky + (p_2 + p_4) \cos \pi (2ky + h + k) + i (p_1 - p_3) \operatorname{Sin} 2\pi ky + i (p_2 - p_4) \operatorname{Sin} \pi (h + k + 2ky).$$

Let the spins of atoms above the ones with Z = 0 be mp_i where $m = \pm 1$, then,

$$F_{magnetic} = (p_1 + p_3) \cos 2\pi ky + (p_2 + p_4) \cos \pi (h + k + 2ky) + i (p_1 - p_3) \operatorname{Sin} 2\pi ky + i (p_2 - p_4) \operatorname{Sin} \pi (h + k + 2ky) + m (p_1 + p_3) \cos 2\pi (ky + 1) + m (p_2 + p_4) \cos \pi (h + k + 2l + 2ky) + m i (p_1 - p_3) \operatorname{Sin} 2\pi (ky + 1) + m i (p_2 - p_4) \operatorname{Sin} \pi (h + k + 2l + 2ky)$$

On the basis of considerations such as allowing or discarding c-centering symmetry or doubling the unit cell along the c-direction, which according to Choh and Stager (1970) are the likely changes to occur in the unit cell and symmetry necessary to describe the magnetic structure, it is possible to construct 35 formally non-equivalent, colinear anti-ferromagnetic arrangements of the spins. Structure factor calculations are described only for two groups of arrangements. One such group enumerated as (a), (b), (c) and (d) is reproduced in figure (X) from Choh and Stager (1970). Only two of these structures, namely (b) and (c), give a strong reflection respectively at 6.9° and 7.1°. In all of these, the unit cell is doubled along the c-axis, but the ones marked with a prime have a unit cell of the same size as the chemical unit cell. Some of the arrangements in the second group consist of different combinations of the above mentioned arrangements and are also shown in the same figure. These configurations give a reflection one-quarter the intensity at 6.9° or 7.1° at these angles whichever is allowed. Simplified expressions for $F_{magnetic}$ with the appropriate conditions imposed on h,k,l for all these arrangements are given in the appendix. It is clear from the appendix that it is mainly in the models VIII to XIII there are somewhat cumbersome conditions imposed on h,k,l for the presence or absence of a particular line. Actual values for $F_{magnetic}$ obtained from all the models, are presented in table I.

VII OBSERVATIONS AND DISCUSSION

The pattern (fig. VI) obtained at 77°K is what was expected on the basis of room temperature X-ray structure determination. The lines predicted at 18.93°, 19.58° and 19.86° are not resolved due to their close proximity, since the resolution of the spectrometer was about 0.7° full width at half height.

As mentioned in an earlier section, extra lines appear in the pattern at 7.1°, 11.2°, 15.65°, etc., on cooling the specimen down to 4.2°K. There is no change in the nuclear peaks except that the ones at 13.7° and 14.2° are resolved. It can also be noticed in fig. (VII) that the curve obtained at 4.2°K lies, except around the strong extra peaks, below the one at 77°K. This slight decrease in intensity at liquid He temperature can be attributed to the disappearance of contributions to scattering due to two phenomena, namely:

a) Diffuse paramagnetic scattering

b) Thermal diffuse scattering .

Both these effects show angular dependence. The former i.e. diffuse paramagnetic scattering diminishes with increase in Bragg angle, whereas, thermal contribution increases with increase in the angle.

The magnetic character of the extra lines appearing at 4.2°K is confirmed by the plot (fig. IX) of intensity versus rise in temperature. There is a decrease in the number of neutrons reflected at 7.1° as the temperature rises. Eventually the extra lines disappear. Allowing for the background scattering, one can roughly estimate the

transition or Néel temperature to be around (13 ± 3)°K; a value found by earlier workers from susceptibility measurements.

It was stated earlier that 35 spin configurations, which were non-equivalent, colinear and antiferromagnetic, were possible. Twenty-two of these did not predict a strong line either at 6.9° or at 7.1°. This leaves us with 13 arrangements. Of these 13, six, which are depicted in fig. (X) as (a',c'), etc., can be discarded just by inspection of table I. For example, a strong line is predicted at 10.46° on (Q), but there is no indication of its presence at all. Of the remaining seven, only two, namely (b) and (c') predict a strong line at 6.9° and 7.1° respectively. A closer examination of the available data, however, reveals overwhelming evidence for (c') as described in the following:

a) According to the changes occurring in the lattice parameters at low temperatures, there should be a slight shift to the right in the pattern. From fig.(VIII) it is clear that lines predicted on (c') show such a consistent shift. Both the intense peaks (010) and (011) appear approximately at the expected angles with the shift to the right.

b) In the case of (c') all the predicted lines can either be clearly observed or there is some indication of their presence where overlap takes place. On the other hand, lines expected on (b) at 12.64°, 14.65°, 18.67° are not observed. On the basis of structure factor (table I) and q^2 (table IA) calculations, one could argue that the first two peaks are very weak and hence unobservable. The remaining two lines respectively at 18.67° and 20.74° are, however, strong and should be detectable even after making allowance for decrease

in intensity due to $\underline{k}$ not lying in the reflecting planes. In constrast, although the lines predicted on (c') at 17.06° 20.2°, 20.73° and 21.37° do not stand out unambigously, but a close scrutiny of the pattern indicates their presence. It should be borne in mind that the lines at 17.06° and 21.37° are weak ones.

It has not been possible to index the line observed at 11.2°. None of the models predicts a line at this angle. It may have originated either as a result of some spurious scattering or due to small distortions taking place in the cell at low temperature. The latter phenomenon is known to occur in other pyrophosphates.

The magnetic unit cell of the chosen model i.e. (c') is drawn in figure (XI) and the observed and calcultaed intensities of the lines are tabulated in table II. There is reasonable agreement between the two. Only the observed intensity of the (010) line is not within error, and is presumably due to extinction effects in the peak. It should also be noticed that the magnetic unit cell is the same size as the chemical unit cell, and is not doubled along the c-axis. The c-centering symmetry, a possibility that seemed to exist on the basis of the NMR studies, is lost.

In conclusion it can be said that $Mn_2P_2O_7$ has a magnetic structure which consists of ferromagnetic sheets of atoms lying approximately in the a-c plane. The moments in each sheet are aligned antiferromagnetically to the moments in the adjoining sheets. As far as the direction of the spins is concerned, neutron data is consistent with the spins being at an angle of 23° from the a-axis in the a-c plane as found by Atkinson and Stager.

While calculating expected intensities, use was made of the expression, $q^2 = 1-(\underline{\epsilon}.\underline{k})^2$ (Section II) which takes the direction of spins into account. As said earlier, the agreement between observed and calculated intensities was reasonable and hence the consistency with the neutron data.

To confirm the angle with some precision, more work, probably with a single crystal, will be required.

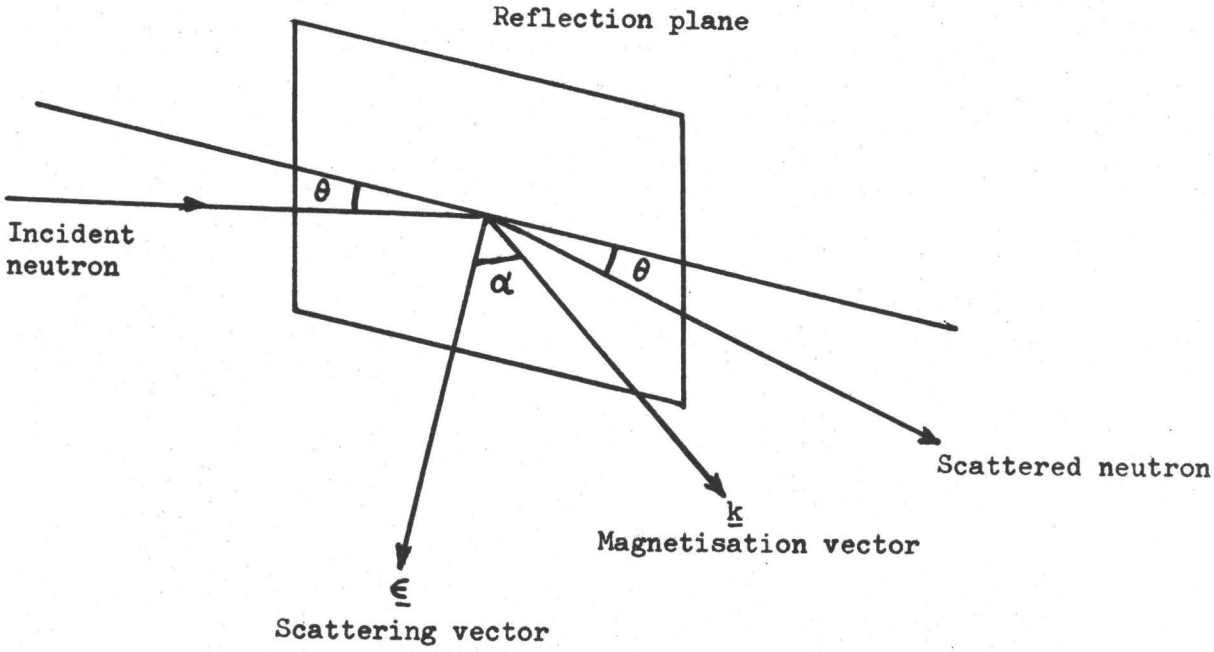

Figure 1: Identification of the unit vectors $\underline{\in}$ and $\underline{k}$ used in the discussion of magnetic scattering. The magnetic interaction vector q is defined as $\underline{\in}(\underline{\in}.\underline{k})-\underline{k}$, so that $\underline{q}$ lies in the plane of $\underline{\in}$, $\underline{k}$ and is perpendicular to $\underline{\in}$. (Bacon: page 161).

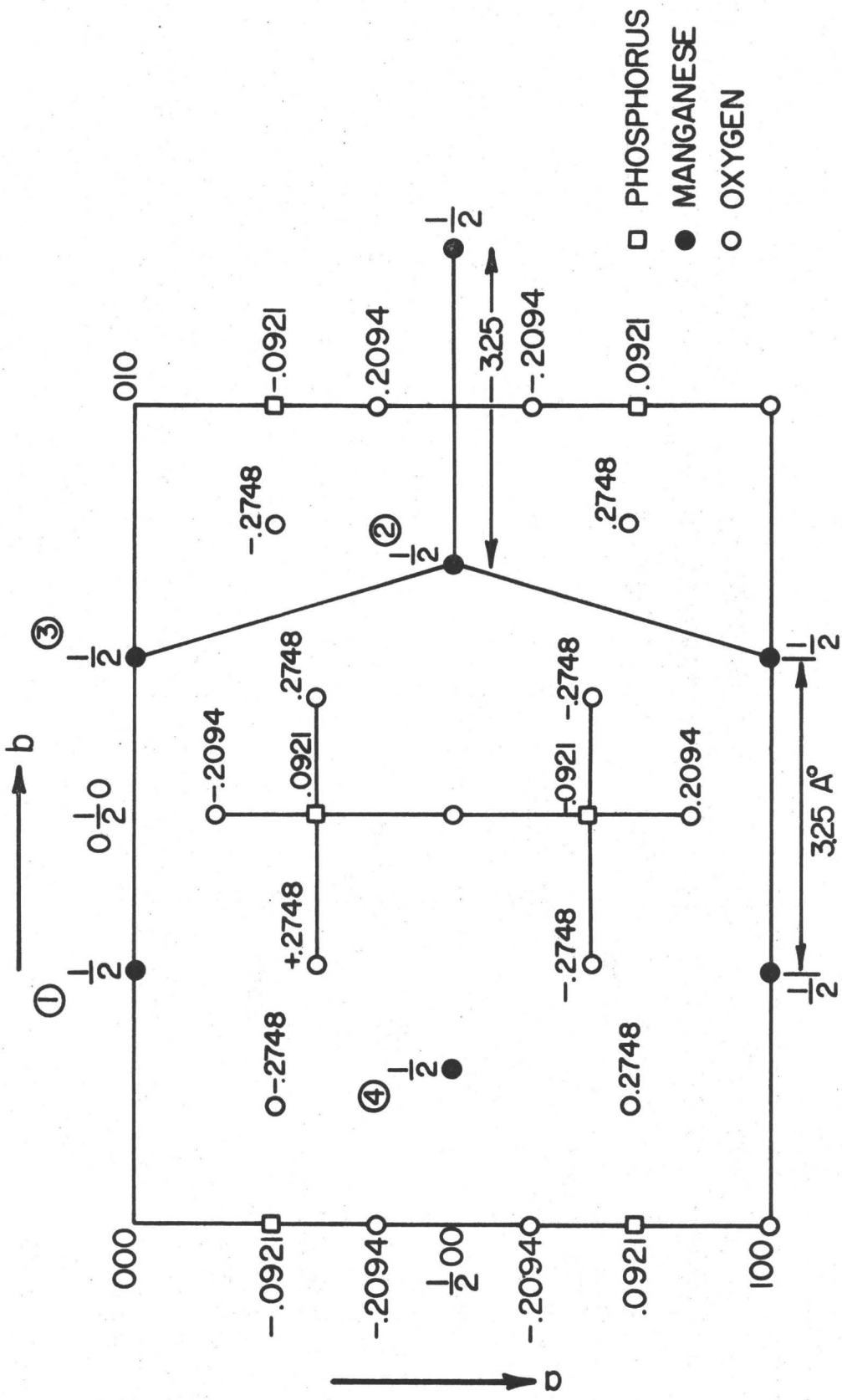

Figure II: Projection of the chemical unit cell on the (a,b) plane. Fractional distances of different atoms are also shown.

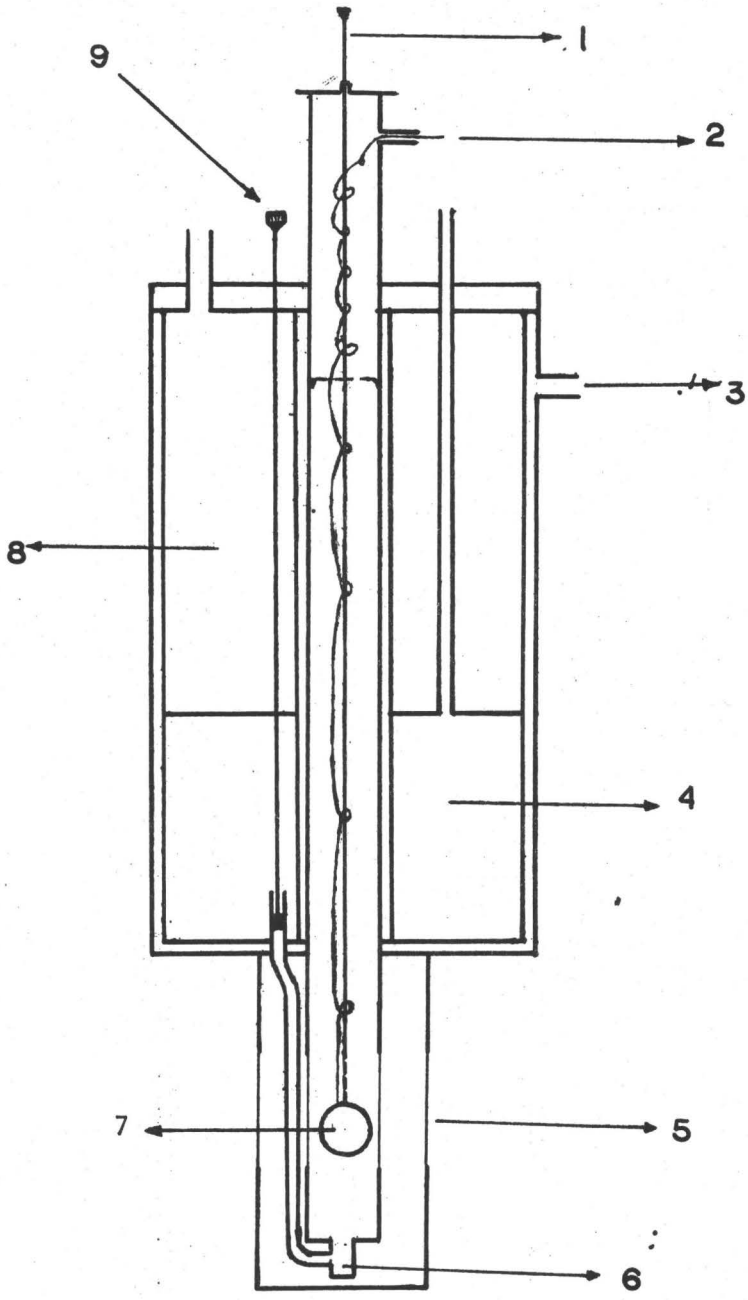

Figure III: An outline of the cryostat showing its various components. (1) Removable Rod (RR): (2) Copper Constantan thermocouple: (3) Vacuum/Relief Valve: (4) Liquid Helium tank: (5) Thinly machined Aluminium section of the tail assembly: (6) Diffuser: (7) Sample container (details in figure IV): (8) Liquid Nitrogen tank: (9) Valve to let liquid Helium into the section containing the sample container.

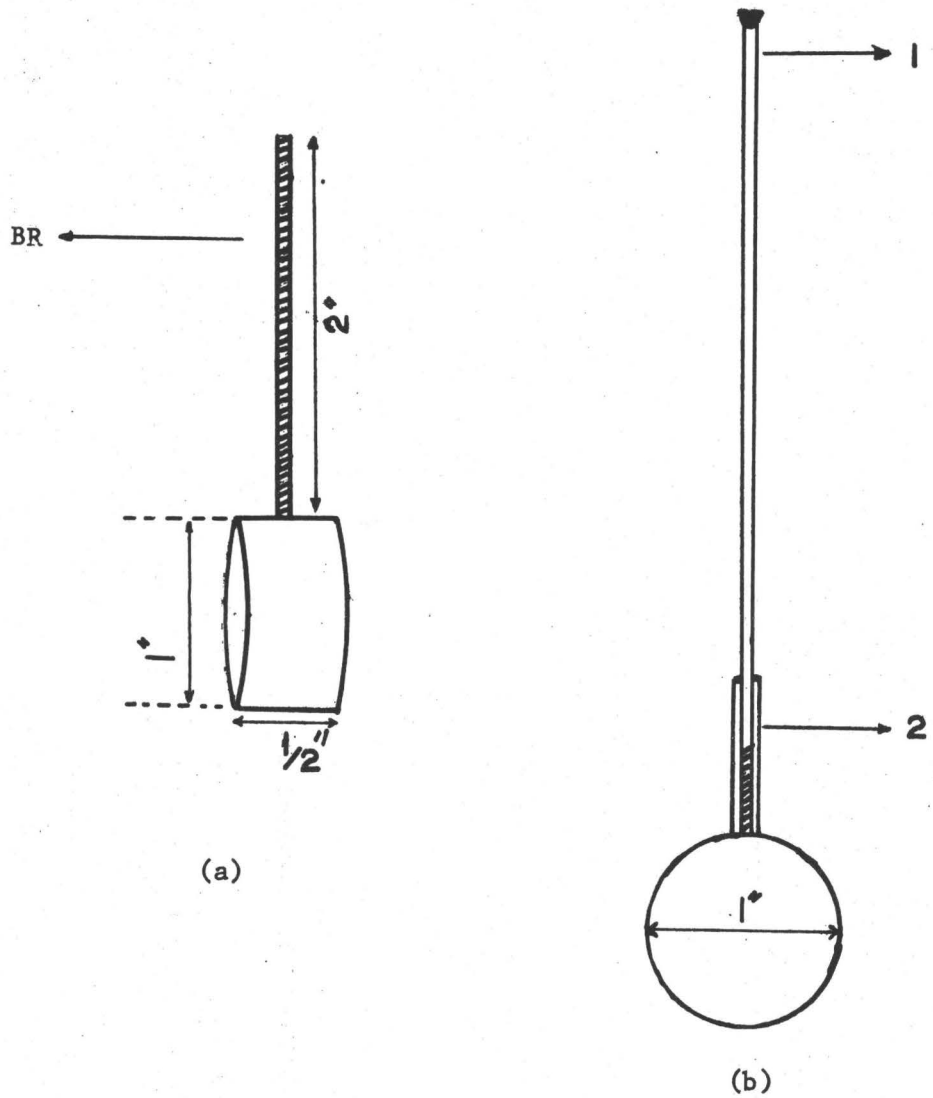

Figure IV: (a) A sketch of the sample holder showing the dimensions of the Aluminium container along with the 2 in. long threaded brass rod (BR) attached to it.
(b) The container is shown attached to the removable rod (RR) in the cryostat. (1) RR: (2) Cadmium Shielding.

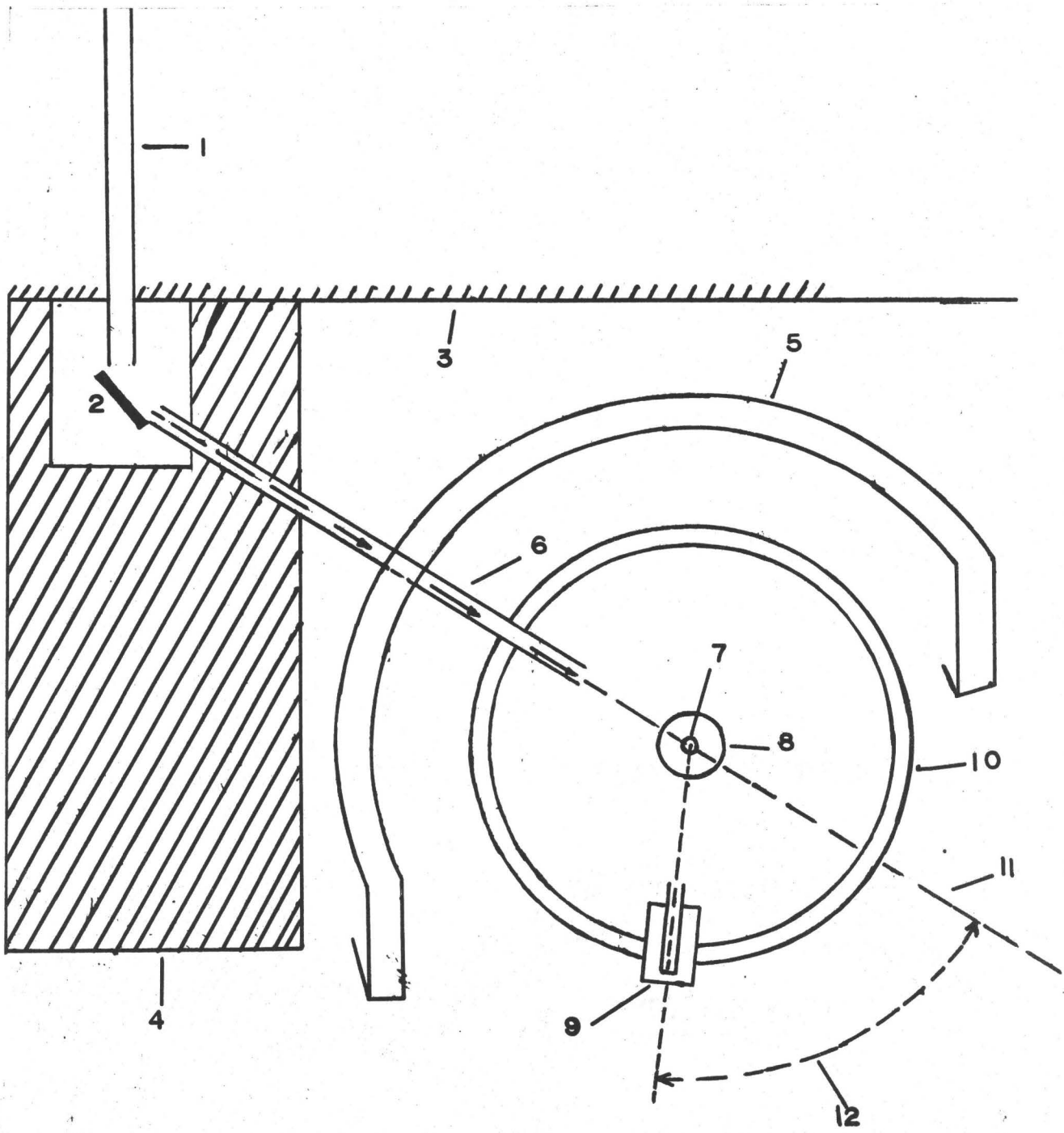

Figure V: A layout of the McMaster University triple axis spectrometer. (1) Collimator: (2) Monochromator Crystal: (3) Reactor face: (4) Concrete and Water Shielding: (5) Water tank, Cadmium Sheet and Wax Shielding: (6) Neutron beam tube: (7) Sample (powder): (8) Spectrometer table: (9) Detector counter: (10) Spectrometer base: (11) Straight-through position: (12) Angle of Scattering 2θ(°).

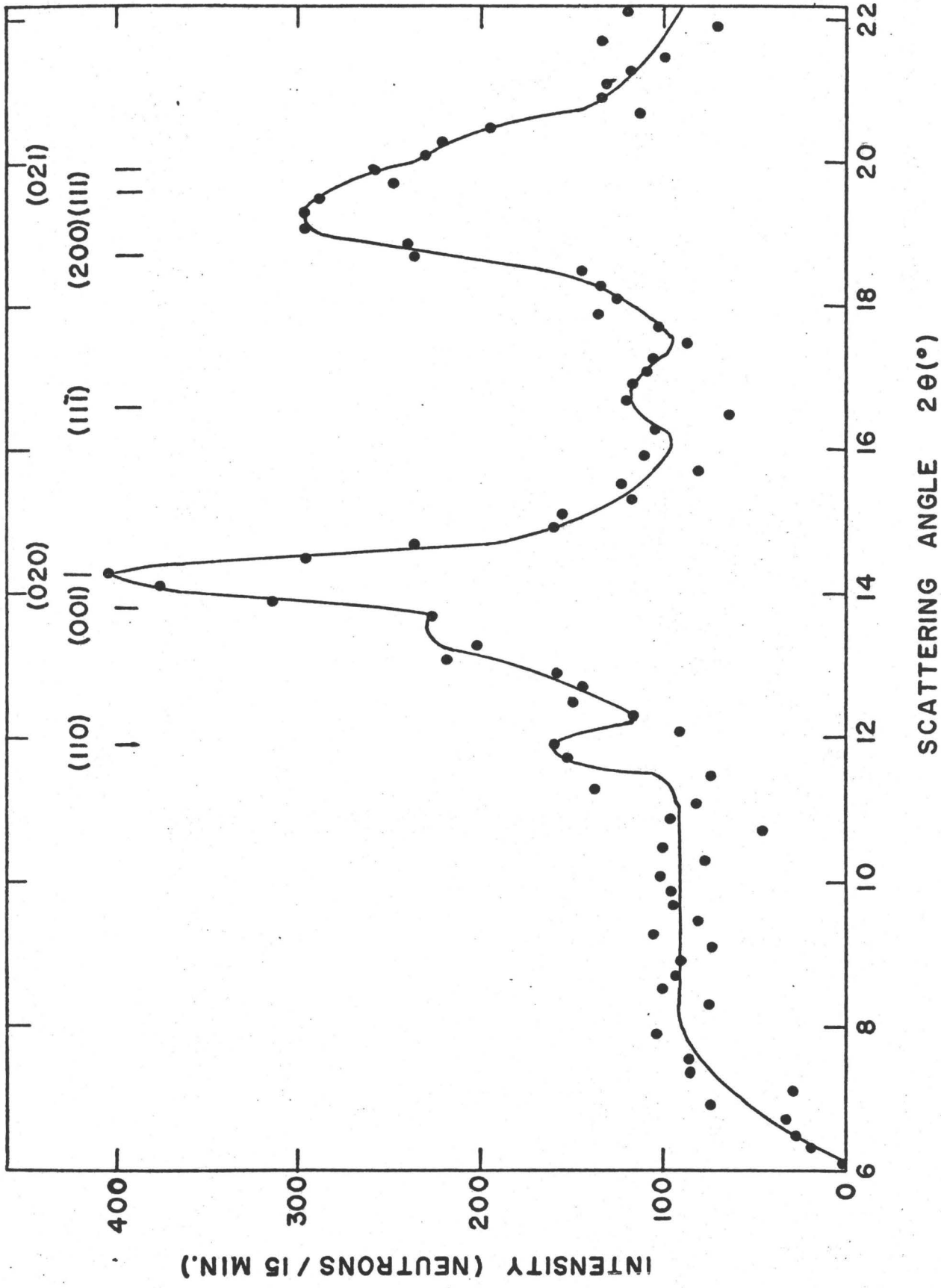

Figure VI: Neutron powder pattern from $Mn_2P_2O_7$ at 77°K. The pattern is that expected on the basis of the room temperature X-ray structure determination.

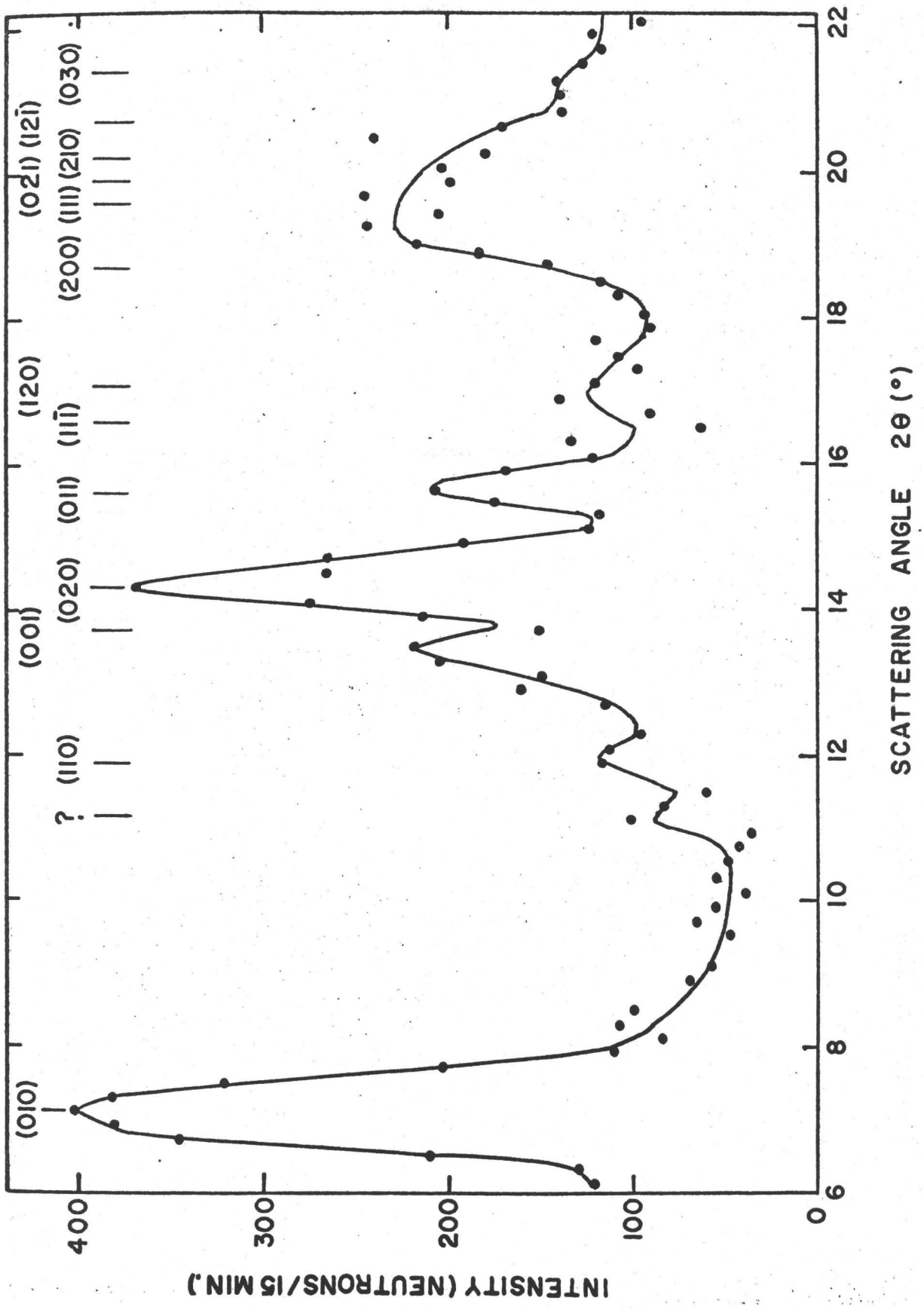

Figure VII: Neutron powder pattern from $Mn_2P_2O_7$ at 4.2°K. The extra lines relative to the 77°K pattern indicate the presence of an ordered antiferromagnetic structure.

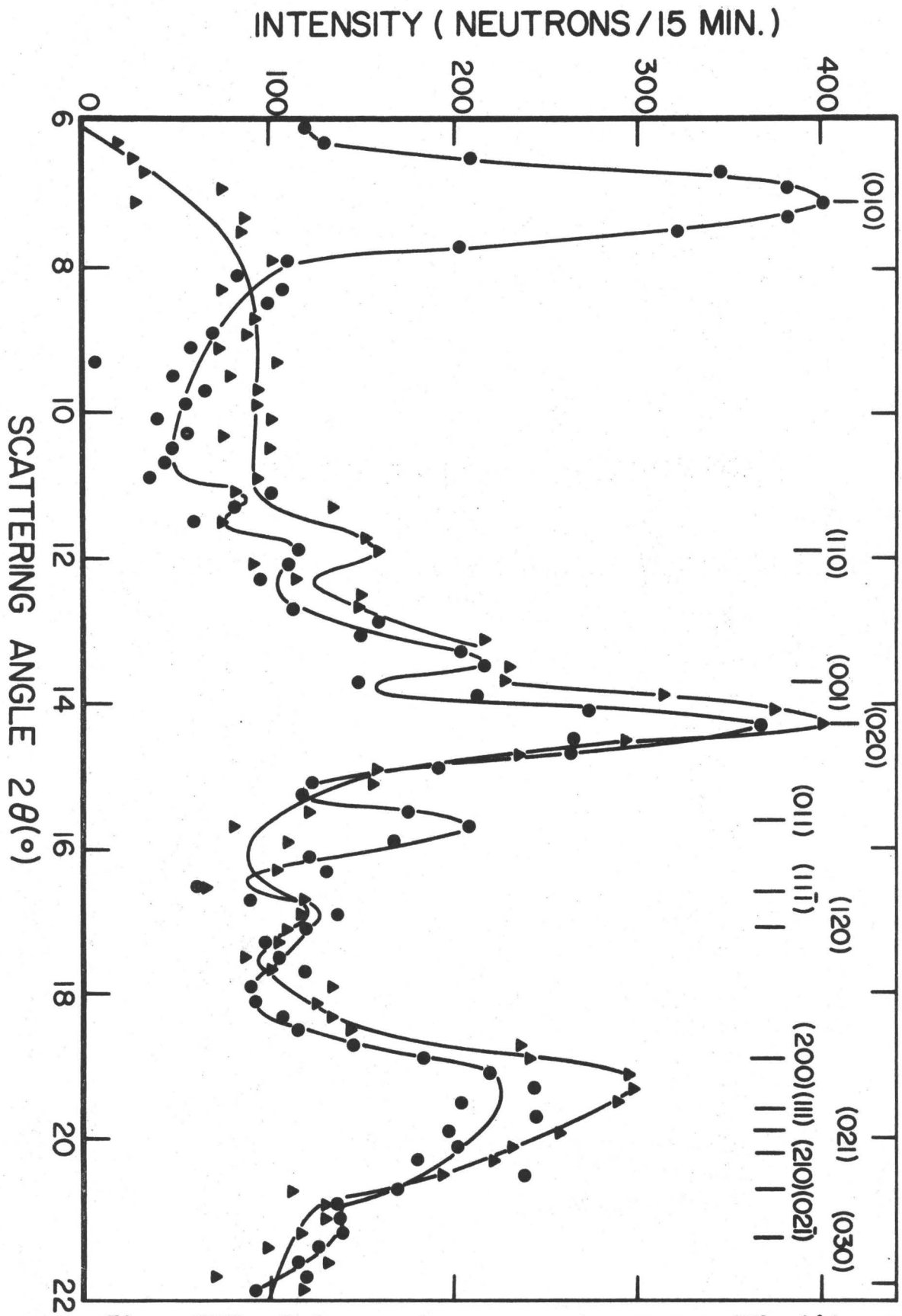

Figure VIII: Neutron powder patterns from $Mn_2P_2O_7$ 77°K (▲) and 4.2°K (●). A direct comparison of the two patterns indicates the ordering at 4.2°K that has taken place in the structure.

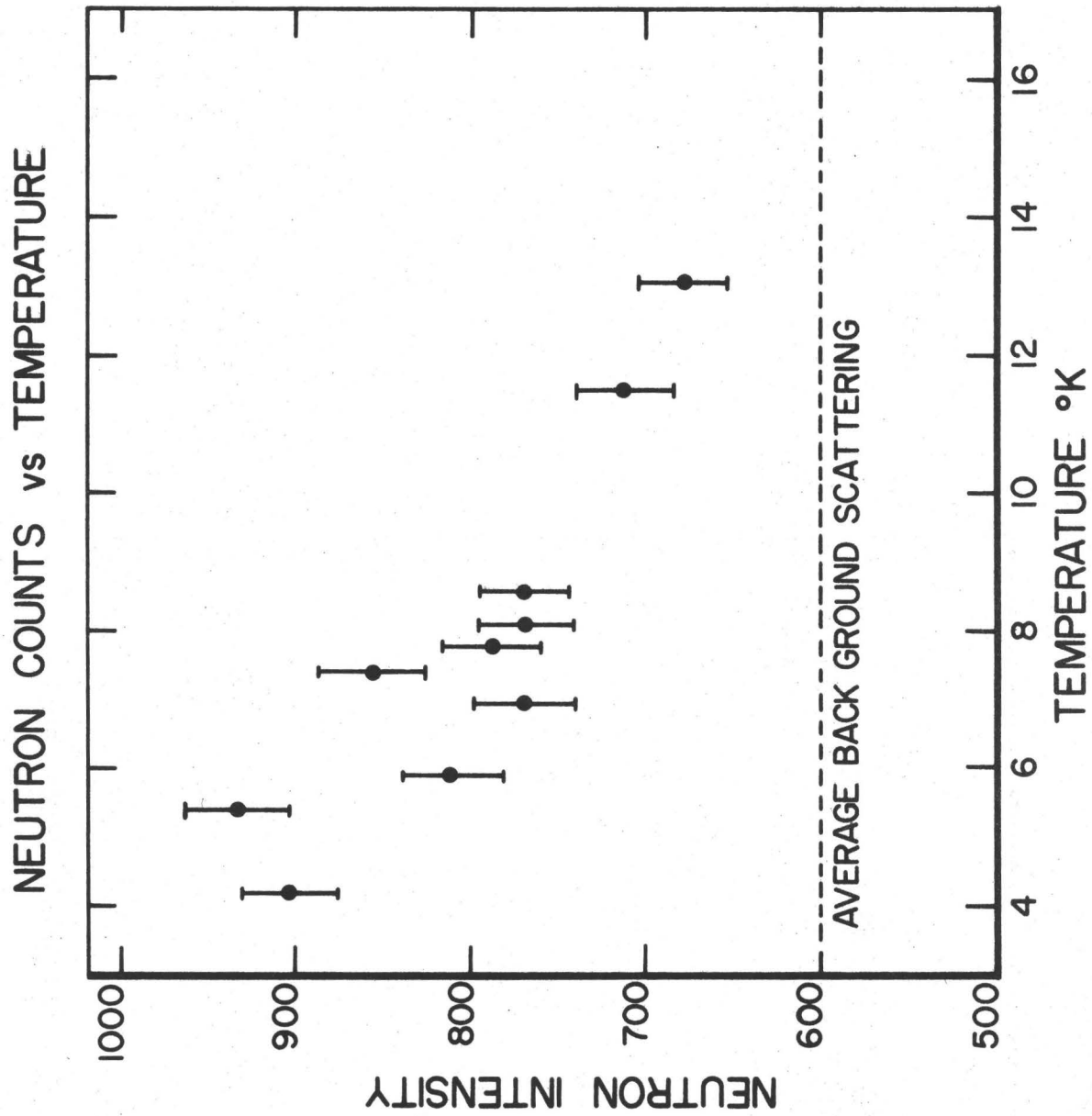

Figure IX: Determination of transition temperature. The sample was cooled down to 4.2°K. The counter was placed at an angle of 7.1°. Temperature was allowed to rise and a plot of number of neutrons scattered vs. temperature was obtained. The horizontal line is the average level of background counts. The transition temperature $\approx (13 \pm 3)$°K.

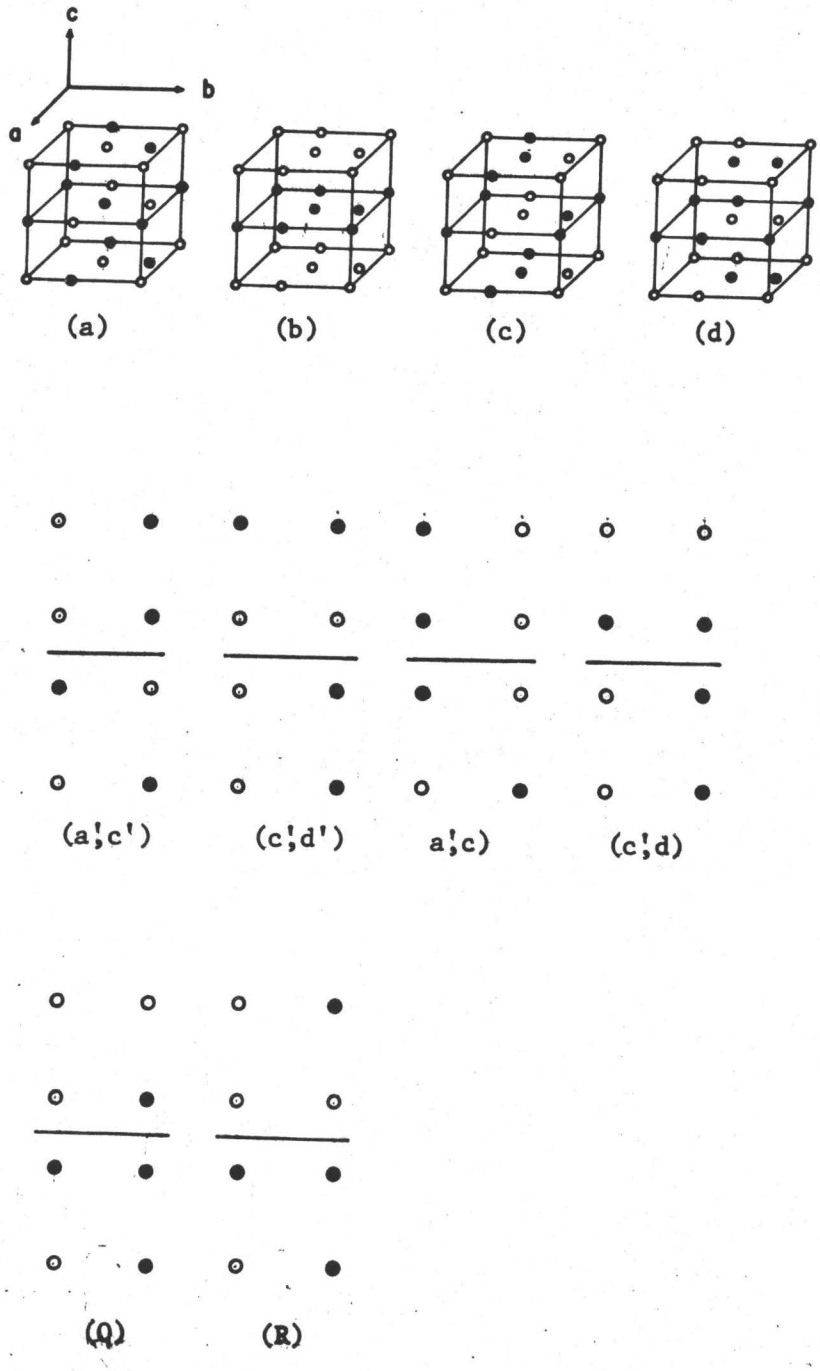

Figure X: Possible antiferromagnetic spin arrangements in $Mn_2P_2O_7$. Diagrams (a), (b), (c) and (d) show a magnetic unit cell double the size of the chemical unit cell. The cell is doubled along the c-axis. (a',c') (c',d'), etc. show the other possible spin configurations. Prime indicates an arrangement in which c-axis is not doubled. The open circles are Manganese atoms with their spins pointing in a direction opposite to that on the atoms shown as solid circles.

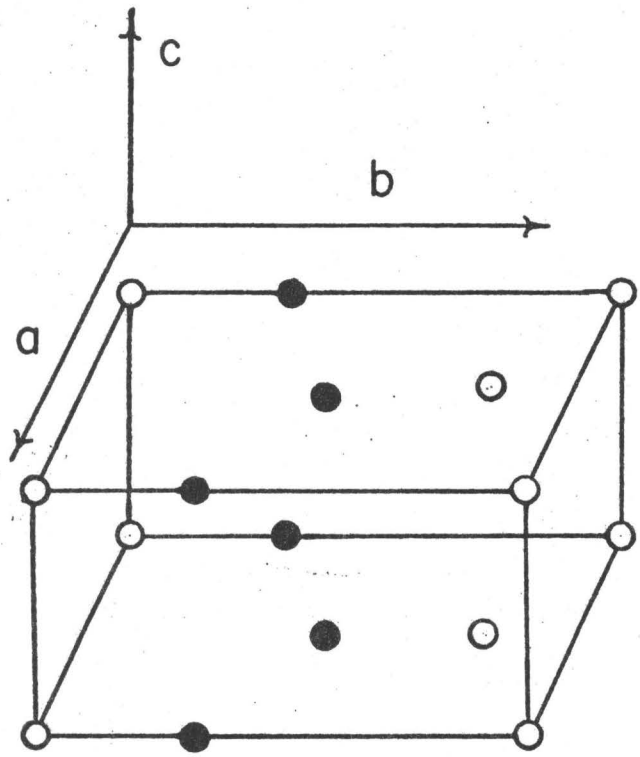

Figure XI: The antiferromagnetic spin arrangement of $Mn_2P_2O_7$. Manganese atoms marked with open circles have spins which point at about 23° to the a axis in the a,c plane. Manganese atoms marked with filled circles have spins pointing in opposite directions to the atoms marked with open circles.

TABLE I

Calculated values of d_{hkl} interplanar spacing, corresponding Bragg angle $2\theta(^\circ)$, magnetic and nuclear structure factors for various (hkl) planes.

* Magnetic structure factor = 8p x the value given in the table.

p is as defined in Section II, equation (iii).

INDEX h k l	d_{hkl} (A°)	EXPECTED BRAGG ANGLE (2θ°)	STRUCTURE FACTOR MAGNETIC MODEL (a)	(a')	(b)	(c)	(c')	(d)	(d')	NUCLEAR
0 0 $\frac{1}{2}$	8.8535	6.88	0	0	1.00	0	0	0	0	0
0 1 0	8.5793	7.12	0	0	0	0	0.927	0	0.374	0
1 0 0	6.4608	9.42	0	0	0	0	0	0	1.000	0
0 1 $\frac{1}{2}$	6.1610	9.94	0	0	0	0.927	0	0.374	0	0
1 0 $\bar{\frac{1}{2}}$	5.8350	10.46	0	0	0	0	0	1.00	0	0
1 1 0	5.1610	11.86	0	0.927	0	0	0	0	0	1.05
1 1 $\bar{\frac{1}{2}}$	4.8246	12.64	0.927	0	0.374	0	0	0	0	0
1 0 $\frac{1}{2}$	4.7644	12.80	0	0	0	0	0	1.00	0	0
0 0 1	4.4271	13.78	0	0	0	0	0	0	0	4.23
0 2 0	4.2895	14.24	0	0.695	0	0	0	0	0	5.26

TABLE I (Continued)

INDEX h k l	d_{hkl} (A°)	EXPECTED BRAGG ANGLE (2θ°)	STRUCTURE FACTOR MAGNETIC MODEL (a)	(a')	(b)	(c)	(c')	(d)	(d')	NUCLEAR
1 1 ½	4.1651	14.65	0.927	0	0.374	0	0	0	0	0
1 0 $\bar{1}$	4.0723	14.97	0	0	0	0	0	0	1.000	0
0 1 1	3.9342	15.50	0	0	0	0	0.927	0	1.000	0
0 2 ½	3.8604	15.80	0.695	0	0.720	0	0	0	0	0
1 1 $\bar{1}$	3.6789	16.60	0	0.927	0	0	0	0	0	1.71
1 2 0	3.5736	17.06	0	0	0	0	0.695	0	0.72	0
1 2 $\bar{½}$	3.4563	17.66	0	0	0	0.695	0	0.72	0	0
1 0 1	3.3400	18.30	0	0	0	0	0	0	1.00	0
2 0 $\bar{½}$	3.2765	18.67	0	0	1.00	0	0	0	0	0
2 0 0	3.2299	18.93	0	0	0	0	0	0	0	6.42
1 2 ½	3.1879	19.10	0	0	0	0.695	0	0.72	0	0
1 1 1	3.1122	19.58	0	0	0	0	0.927	0	0	1.11
0 2 1	3.0806	19.86	0	0.695	0	0	0	0	0	2.68
2 1 $\bar{½}$	3.0501	20.03	0	0	0	0.927	0	0.374	0	0
2 1 0	3.0232	20.20	0	0	0	0	0.927	0	0.374	0
1 2 $\bar{1}$	2.9533	20.73	0	0	0	0	0.695	0	0.72	0

TABLE I (Continued)

INDEX h k l	d_{hkl} (A°)	EXPECTED BRAGG ANGLE 2θ°	STRUCTURE FACTOR MAGNETIC MODEL (a)	(a')	(b)	(c)	(c')	(d)	(d')	NUCLEAR
0 0 $^{3}/_{2}$	2.9513	20.74	0	0	1.00	0	0	0	0	0
1 0 $^{\bar{3}}/_{2}$	2.9268	20.90	0	0	0	0	0	1.00	0	0
0 3 0	2.8596	21.37	0	0	0	0	0.407	0	0.913	0

*In the following Magnetic Structure factor values are to be multiplied by 4P. P is as defined earlier.

h k l	d_{hkl} A°	Predicted Bragg Angle (2θ)°	Magnetic Structure factor					
			Model					
			(a',c')	(c,d')	(a',c)	(c',d)	(Q)	(R)
0 0 $\frac{1}{2}$	8.8535	6.88	0	0	0	0	1	1
0 1 0	8.5793	7.12	0	(0.374-.927i)	.927	.374-.927i	.927	.374
1 0 0	6.4608	9.42	0	1	0	0	0	0
0 1 $\frac{1}{2}$	6.1610	9.94	0	.927(1-i)	.927	.927(1+i)	.374	0
1 0 $\frac{\bar{1}}{2}$	5.8350	10.46	0	0	0	1	1	0
1 1 0	5.1610	11.86	0	0	.927	0	.927	1.854
1 1 $\frac{\bar{1}}{2}$	4.8246	12.64	1.854	0	.927	0	.374	.374
1 0 $\frac{1}{2}$	4.7644	12.80	0	0	0	1	1	0
0 0 1	4.4271	13.78	0	0	0	0	0	0
0 2 0	4.2895	14.24	0	0	.695	0	.695	1.390
1 1 $\frac{1}{2}$	4.1651	14.65	1.390	0	.927	0	.374	.374
1 0 $\bar{1}$	4.0723	14.97	0	0	0	1	0	0
0 1 1	3.9342	15.50	0	.927(1-i)	.927	.927(1+i)	.927	0
0 2 $\frac{1}{2}$	3.8604	15.80	1.390	0	.695	0	.719	.695
1 1 $\bar{1}$	3.6789	16.60	0	0	.927	0	.927	1.854
1 2 0	3.5736	17.06	0	.695(1-i)	.695	.695(1+i)	.695	0
1 2 $\frac{\bar{1}}{2}$	3.4563	17.66	0	.695(1+i)	.695	.719-.695i	.719	0
1 0 1	3.3400	18.30	0	0	0	1	0	0
2 0 $\frac{\bar{1}}{2}$	3.2765	18.67	0	0	0	0	1	1

*In the following Magnetic Structure factor values are to be multiplied by 4P. P is as defined earlier.

h k l	d_{hkl} A°	Predicted Bragg Angle (2θ)°	Magnetic Structure factor					
			Model					
			(a',c')	(c,d')	(a',c)	(c',d)	(Q)	(R)
2 0 0	3.2299	18.93	0	0	0	0	0	0
1 2 $\frac{1}{2}$	3.1879	19.10	0	.695(1+i)	.695	.719+.695i	.695	0
1 1 1	3.1122	19.58	0	0	.927	0	.927	1.854
0 2 1	3.0806	19.86	0	0	.695	0	.695	1.390
2 1 $\frac{-1}{2}$	3.0501	20.03	0	.927(1-i)	.927	.374-.927i	.927	0
2 1 0	3.0232	20.20	0	.927(1-i)	.927	.374+.927i	.927	0
1 2 1	2.9533	20.73	0	.695(1+i)	.695	.719-.927i	.695	0
0 0 $\frac{3}{2}$	2.9513	20.74	0	0	0	0	1	1
1 0 $\frac{3}{2}$	2.9268	20.90	0	0	0	1	1	0
0 3 0	2.8596	21.37	0	.407(1+i)	.407	.913+.407i	.407	0

TABLE IA

Calculated Values of q^2.

$\underline{q}$ is the magnetic interaction vector defined in figure I.

Index h,k,l			$q^2 = 1-(\underline{\epsilon}.\underline{k})^2$
0	0	$\frac{1}{2}$	0.84
0	1	0	1.00
1	0	0	0.17
0	1	$\frac{1}{2}$	1.00
1	0	$\bar{\frac{1}{2}}$	0.60
1	1	0	0.74
1	1	$\bar{\frac{1}{2}}$	0.88
1	0	$\frac{1}{2}$	0.00
0	0	1	0.83
0	2	0	1.00
1	1	$\frac{1}{2}$	0.62
1	0	$\bar{1}$	0.87
0	1	1	0.98
0	2	$\frac{1}{2}$	1.00
1	1	$\bar{1}$	0.97
1	2	0	0.94
1	2	$\bar{\frac{1}{2}}$	0.98
1	0	1	0.13
2	0	$\bar{\frac{1}{2}}$	0.62
2	0	0	0.17

Continued

TABLE IA (Continued)

Index h,k,l			$q^2 = 1-(\underline{\epsilon}.\underline{k})^2$
1	2	$\frac{1}{2}$	0.90
1	1	1	0.57
0	2	1	1.00
2	1	$\bar{\frac{1}{2}}$	0.62
2	1	0	0.47
1	2	$\bar{1}$	1.00
0	0	$3/2$	0.83
1	0	$\bar{3}/2$	0.97
0	3	0	1.00

Table II.

Observed and calculated intensities of powder lines from manganese pyrophosphate.

Peak	Type	Observed Intensity	Calculated Intensity
010	M	35 ± 7	53
110	N	6.3± 3	3.3
001	N	48 ± 8	53
020	N	82 ± 12	82
011	M	39 ± 10	37
$11\bar{1}$	N	12 ± 7	9
120	M	9 ± 7	13

N represents a nuclear reflection and M a magnetic one

The calculated intensities are normalised to the observed intensity of the (020) peak. The observed intensities quoted are the areas of the peaks multiplied by the geometric factor $\sin^2 2\theta$ (Bacon 1962, p. 96).

APPENDIX

In the following, simplified expressions have been derived for $F_{magnetic}$ for all the possible magnetic models of $Mn_2P_2O_7$, mentioned in section VI.

i) Structure (a):

$$p_1 = p_2 = -p_3 = -p_4 = p$$

$$m = -1$$

$$\left|F_{magnetic}\right| = 8p \operatorname{Sin} \pi l \cos \frac{\pi}{2}(h + k) \operatorname{Sin} 2\pi ky$$

With l half-integral, (h + k) even.

ii) Structure (a'):

$$p_1 = p_2 = -p_3 = -p_4 = p$$

$$m = 1$$

$$\left|F_{magnetic}\right| = 8p \cos \pi l \cos \frac{\pi}{2}(h + k) \operatorname{Sin} 2\pi ky$$

With l integral, (h + k) even.

iii) Structure (b):

$$p_1 = p_2 = p_3 = p_4 = p$$

$$m = -1$$

$$\left|F_{magnetic}\right| = 8p \operatorname{Sin} \pi l \cos 2\pi ky \operatorname{Cos} \frac{\pi}{2}(h + k)$$

With l half-integral, (h + k) even.

iv) Structure (c):

$$p_1 = p_4 = -p_2 = -p_3 = p$$

$$m = 1$$

$$\left|F_{magnetic}\right| = 8\, p \cos \pi l \operatorname{Sin} \frac{\pi}{2}(h + k) \operatorname{Sin} 2\pi ky$$

With l integral, (h + k) odd.

v) Structure (c'):

$$p_1 = p_4 = -p_2 = -p_3 = p$$

$$m = 1$$

$$\left|F_{magnetic}\right| = 8p \cos \pi l \, \text{Sin} \, \frac{\pi}{2} (h + k) \, \text{Sin} \, 2\pi ky$$

l integral, (h + k) odd.

vi) Structure (d):

$$-p = -p_3 = p_2 = p_4 = p$$

$$m = -1$$

$$\left|F_{magnetic}\right| = 8p \, \text{Sin} \, \pi l \cos 2\pi ky \, \text{Sin} \, \frac{\pi}{2} (h + k)$$

l half-integral, (h + k) odd.

vii) Structure (d'):

$$-p_1 = -p_3 = p_2 = p_4 = p$$

$$m = 1$$

$$\left|F_{magnetic}\right| = 8p \cos \pi l \cos 2\pi ky \, \text{Sin} \, \frac{\pi}{2} (h + k)$$

with l integral, (h + k) odd.

viii) Structure (a',c'):

$$p_1 = p_2 = -p_3 = -p_4 = p; \quad Z = 0$$

$$-p_1 = p_2 = p_3 = -p_4 = p; \quad Z = 1$$

For l half integral, (h + k) even

$$\left|F_{magnetic}\right| = 8p \, \text{Sin} \, \pi l \cos \pi(2ky + 1) \cos \pi \frac{h + k}{2}$$

ix) Structure (c',d'):

$$-p_1 = p_2 = p_3 = -p_4 = p; \quad Z = 0$$

$$p_1 = -p_2 = p_3 = -p_4 = p; \quad Z = 1$$

$$\left|F_{magnetic}\right| = 4p \, \text{Sin} \, 2\pi ky - i \cos \pi(2ky + \frac{h + k}{2}) \, \text{Sin} \, \frac{\pi}{2} (h + k)$$

i.e. k integral or half-integral; (h + k) odd.

x) Structure (a',c):

$$p_1 = p_2 = -p_3 = -p_4 = p; \quad Z = 0$$

$$p_1 = -p_2 = -p_3 = p_4 = p; \quad Z = 1$$

$$\left|F_{magnetic}\right| = 4p \cos \pi (2ky + 1) \operatorname{Sin} \pi l$$

for l half integral; (h + k) even or odd

$$\left|F_{magnetic}\right| = 4p \operatorname{Sin} \pi (2ky + 1) \cos \pi l$$

xi) Structure (c',d):

$$-p_1 = p_2 = p_3 = -p_4 = p; \quad Z = 0$$

$$-p_1 = p_2 = -p_3 = p_4 = p; \quad Z = 1$$

$$F_{magnetic} = 4p \left[\operatorname{Sin} \pi (2ky + \frac{h + k}{2}) + i \cos \pi (2ky + \frac{h + k}{2})\right]$$

$$\operatorname{Sin} \pi \frac{h + k}{2}$$

l integral or half-integral; (h + k) odd.

The following two structures are not a combination of the ones mentioned previously. These give lines at both 6.9° and 7.1° and are denoted as Q or R.

xii) Structure (Q):

$$p_1 = p_2 = p_3 = -p_4 = p; \quad Z = 0$$

$$-p_1 = p_2 = -p_3 = -p_4 = p; \quad Z = 1$$

l half integral; (h + k) even or odd

$$\left|F_{magnetic}\right| = 4p \operatorname{Sin} \pi l \operatorname{Sin} \pi (2ky + 1)$$

For l integral; (h + k) even or odd

$$\left|F_{magnetic}\right| = 4p \operatorname{Sin} 2\pi ky \cos \pi l$$

xiii) Structure (R):

$$p_1 = p_2 = p_3 = -p_4 = p; \quad Z = 0$$

$$-p_1 = -p_2 = p_3 = -p_4 = p; \quad Z = 1$$

$$\left|F_{magnetic}\right| = 4p \text{ Sin } \pi (2ky + 1) \text{ Sin } \pi (1 + \frac{h + k}{2})$$

i.e. 1 half-integral; (h + k) even

$$\left|F_{magnetic}\right| = 4p \text{ Sin } \pi (2ky + 1 + \frac{h + k}{2}) \text{ Sin } \pi (1 + \frac{h + k}{2})$$

i.e. 1 integral; (h + k) odd

$$\left|F_{magnetic}\right| = 8p \text{ Sin } \pi (2ky + 1) \cos \pi l \cos \pi \frac{h + k}{2}$$

i.e. 1 integral; (h + k) even.

BIBLIOGRAPHY

Anderson, P. W. In. Magnetism Vol. I, P. 25, Acad. Press, 1963.

Atkinson, R. J. & Stager, C. V., 1969, Can. J. Phys. 47, 1557.

Bacon, G. E., 1962, Neutron Diffraction (Oxford University Press, Oxford) Second Edition.

Brockhouse, B. N., Dewit, G. A., Hallman, E. D. and Rowe, J. M., 1968, Neutron Inelastic Scattering, Vol. II, IAEA, Vienna, P. 259.

Calvo, C. V., Tondon, V. K., Private Communication.

Chambers, J. G., Datars, W. R. and Calvo, C. 1964, J. Chem. Phys. 41, 806.

Choh, S. G. and Stager, C. V. 1970, Can. J. Phys., 48, 521.

de Gennes, P. G. Magnetism Vol III, P. 115, Acad. Press, 1963.

Fowlis, D. C. and Stager, C. V., 1969, Can. J. Phys., 47, 371.

Lukaszewicz, K. and Smajkiewicz, R., 1961, Roczniki Chem., 35, 741.

Nagamiya, T., Yosida, K., Kubo, R., 1955, Phil. Marg. Suppl. 4,1.

Shull, C. G. and Smart, J. S., Phys. Rev. 76, 1949, 1256.